Water droplets effects on an airfoil aerodynamic performance

I. Aramendia, U. Fernandez-Gamiz, A. Lopez-Arraiza, M.A. Gomez-Solaetxe, J.M. Lopez-Guede and
J. Sancho

Abstract—Wind turbines do not operate only by the effects of the external airflow but with some adverse atmospheric conditions and environmental agents. Surface contamination, erosion, rain or ice accretion are some of them that contribute to an increase of the roughness in the airfoil and therefore to energy losses. We have developed a Computational Fluid Dynamics (CFD) model to evaluate the fluid film formation over the DU91W(2)250 airfoil at three different angles of attack, zero, four and six degrees respectively, through the Lagrangian Multiphase Model (LMP). The fluid film thickness and its total amount of mass were calculated over time. We observed slight differences in the pressure coefficients in light rainy conditions confirming the sensitive of the airfoils to the appearance of a water film layer on them.

Keywords—Airfoil, multiphase flow, numerical simulation, rain droplets, wind turbines.

I. INTRODUCTION

The depletion of global fossil fuel reserves in the last years has served to focus attention on the development of ecologically compatible and renewable energy sources. Wind is at present the second largest power generating capacity in the European Union after overtaking coal in 2016 [1], showing the significant impact in the last years of research fields such as the active and passive flow control devices [2] and the airfoil designs. However, adverse atmospheric conditions such as surface contamination due to the impact of small insects in the blades, or erosion because of dust particles, lead to undesirable effects on aerodynamic performance. Besides, wind turbines working in cold regions or at high altitudes are exposed to heavy rain and icing condition during winter operation. Parent and Ilinca described the ice accretion effects on wind turbines and the main icing mitigation systems based on two main strategies: anti-icing and de-icing [3]. Investigating the effects of all of these phenomena is necessary to improve the design and performance of wind turbines.

With respect to rain some experimental studies were carried out to check its influence and effects, although most of them on aircraft applications [4]-[7]. Dunham performed several wind-tunnel experimental studies to explore the effect of rain on airfoils [8]. His results showed that rain can act as a surface contaminant, causing early boundary-layer transition for low Reynolds number and natural laminar-flow airfoils. Additionally, he reported that the sensitivity of the airfoil section to rain effects was probably dependent on the wettability of the surface. On the other hand, he also studied high-lift airfoils such as the NACA 64-210 and NACA 0012. They showed different sensitivities to a simulated rain spray. With both airfoils in a flapped configuration, significant reductions in maximum lift capability were noted. In addition, the effect of rain on lift occurred near the region of maximum lift and little effect was observed at lower angles of attack. At present, few experimental studies have been carried out with wind turbine applications. Al et al. [9] performed an experimental procedure to study the effect of rain on vertical axis wind turbines. The rain was simulated by means of spray nozzles mounted in the ceiling of the wind tunnel at several points in the working section. Their results confirmed that rain significantly downgrade the performance with an increasing in the drag and decreasing the power for the equivalent wind speed. Recently, Siddons et al. analyzed the influence of rain droplet impingement on wind turbine materials reaching to the conclusion that the tip speed of the wind turbine is of greater importance when compared to the relevant rainfall conditions as to where the wind turbine is situated [10].

Numerical models through Computational Fluid Dynamics (CFD) provide a useful methodology to study the impingement of rain droplets in an airfoil and to obtain valuable data related with the water-film-layer influence in the aerodynamic performance. Valentine and Decker studied the NACA64-210 airfoil aerodynamic performance and the track of raindrops in

I. Aramendia is with the the University of the Basque Country UPV/EHU. He is now with the Nuclear Engineering and Fluid Mechanics Department, Vitoria-Gasteiz, Alava 01006 Spain (corresponding author to provide phone: +34 945014123; e-mail: inigo.aramendia@ehu.eus).

U. Fernandez-Gamiz is with the University of the Basque Country UPV/EHU. He is now with the Nuclear Engineering and Fluid Mechanics Department, Vitoria-Gasteiz, Alava 01006 Spain (e-mail: unai.fernandez@ehu.eus).

A. Lopez-Arraiza is with the University of the Basque Country UPV/EHU. He is now with the Department of Nautical Science and Marine Systems, Bilbao, Bizkaia 48013 Spain (e-mail: alberto.lopeza@ehu.eus).

M. A. Gomez-Solaetxe is with the University of the Basque Country UPV/EHU. He is now with the Department of Nautical Science and Marine Systems, Bilbao, Bizkaia 48013 Spain (e-mail: miguel.solaetxe@ehu.eus).

J. M. Lopez-Guede is with the University of the Basque Country UPV/EHU. He is now with the Systems Engineering and Automatics Department, Vitoria-Gasteiz, Alava 01006 Spain (e-mail: jm.lopez@ehu.eus).

J. Sancho is with the University of the Basque Country UPV/EHU. He is now with the Nuclear Engineering and Fluid Mechanics Department, Vitoria-Gasteiz, Alava 01006 Spain (e-mail: javier.sancho@ehu.eus).

flow over the airfoil by numerical simulation [11]-[12]. The loss of boundary layer momentum to splashed back droplets was studied. However, the effective roughening of the airfoil surface due to the uneven water film formed was not captured in these studies. Wu et al. [13] explored the aerodynamic penalties of this airfoil due to heavy rain conditions at different angles of attack. A maximum lift coefficient decrease of 13.2% and a maximum drag coefficient increase of 47.6% were observed. A CFD model based on the Lagrangian-Eulerian approach was developed by Cai et al. [14] to assess the performance of the S809 airfoil under rainy conditions. In that research, the mass of the droplets was added to the fluid film as a source term in its continuity equation by coupling the Lagrangian multiphase model and the Eulerian Volume of Fluid (VOF) methods. Their results showed a considerable increase in drag and lift degradation. Recently, Cohan and Arastoopour [15] have studied the effect of rain in this airfoil for different rainfall rates in addition to the effect of surface tension and surface property. Their results showed that surface tension has a dominant effect on the performance of the airfoil and should not be neglected under simulated rainy conditions. They observed that, at low rainfall rates, the performance of the airfoil is highly sensitive to the rainfall rate. However, they reported that if the rainfall rate is high enough to immerse most of the airfoil surface under water, a further increase in the rainfall rate does not have a substantial effect on the performance of the airfoil.

The structure of this work starts with a description of the NREL 5MW reference wind turbine and its airfoil distribution. Then the numerical model is introduced defining the computational domain, the discretization of itself and the physics and boundary conditions. A lift and drag coefficients are obtained for three different angles of attack: zero, four and six degrees, respectively. Then, the effects due to the fluid film thickness and the amount of mass accumulated in the fluid film over time are discussed and the pressure coefficient curves with rain and no rain are compared.

II. NREL 5MW REFERENCE WIND TURBINE

The NREL 5 MW reference wind turbine is being used extensively in studies by the wind energy research community as the one to represent the future offshore HAWT (Horizontal Axis Wind Turbines) [16]. Many different works have been performed based on this wind turbine concept including studies about rotor aerodynamics, controls, offshore dynamics and design code development.

The blade airfoil locations, labeled as r (m) in Table I, are directed along the blade-pitch axis from the rotor center to the blade cross sections [17]. The reported NREL 5MW airfoil distribution is shown in Fig.1. More detailed information on the DU series used in the present study can be found in the work made by Timmer [18]
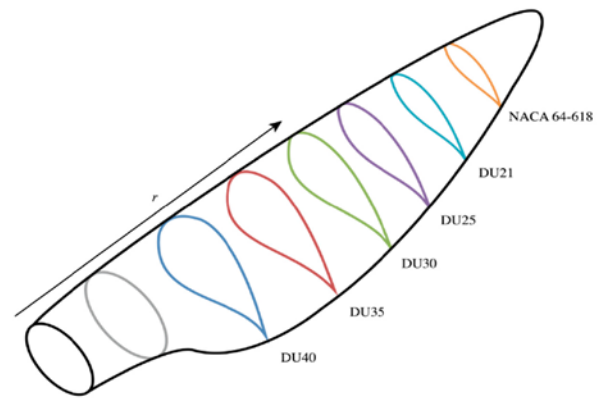

Fig.1 Airfoil distribution along the blade [19]

Station	r (m)	Airfoil
1	2.8667	Cylinder1
2	5.6000	Cylinder1
3	8.3333	Cylinder2
4	11.7500	DU40
5	15.8500	DU35
6	19.9500	DU35
7	24.0500	DU30
8	28.1500	DU25
9	32.2500	DU25
10	36.3500	DU20
11	40.4500	DU20
12	44.5500	NACA64XX
13	48.6500	NACA64XX
14	52.7500	NACA64XX
15	56.1667	NACA64XX
16	58.9000	NACA64XX
17	61.6333	NACA64XX

Table. I Airfoil distribution on the NREL 5 MW blade

III. NUMERICAL MODELING

In the current study, the commercial software STAR-CCM+ (Siemens) [20] has been used for simulating the external airflow and the impingement effects of water droplets and the fluid film formed on a DU91W(2)250, an aerodynamic airfoil developed at Delft University specially for horizontal axis wind turbines.

A. Computational domain and discretization

The computational domain was extended 32 times the airfoil chord length (R=32c). The design and construction of a high quality grid is crucial to the success of the CFD analysis and have the most direct influence on the precision, convergence and time required of the solution. Fig. 2 shows the cell distribution of the computational domain. A two dimensional O-grid was created with about 208.000 structured cells. The mesh was conveniently refined in those regions close to the surface of the airfoil in order to obtain a dimensionless distance less than 1 ($y^+ < 1$) on the airfoil wall, as illustrated in Fig. 3 for the case of alpha 0 degrees.
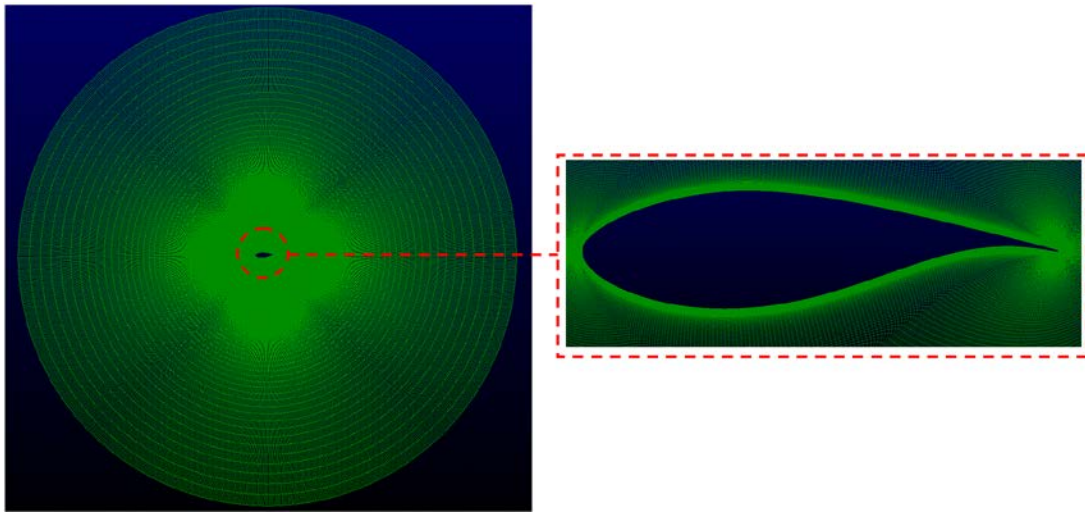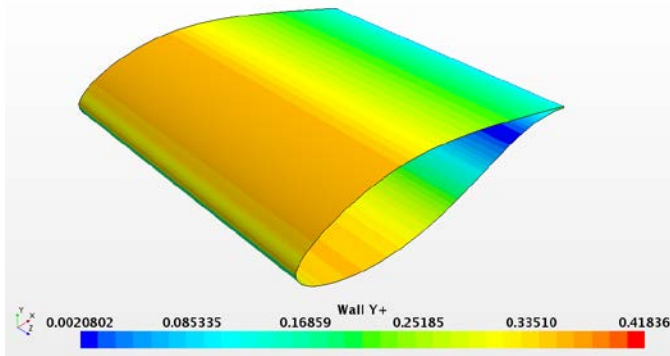
Fig.2 Discretization of the computational domain

Fig.3 Non-dimensional wall y+

B. Physics and numerical models

The CFD code uses discretization methods to convert the continuous system of equations to a set of discrete algebraic equations by means of the Finite Volume Method.

The conservation laws for a continuum can be expressed using an Eulerian approach or a Lagrangian approach. In the Eulerian approach, a given volume represents a portion of space where material can flow through. In the Lagrangian approach, a given volume represents a portion of material in the body, so that an observer follows the material as it moves through space. The governing equations for the *continuous phase* (external airflow) are expressed in Eulerian form and they are modified to take into account the presence of the *dispersed phase* (raindrops). For flows involving a large number of dispersed particles, the total number of particles is represented by a smaller number of computational parcels. Each of these parcels represents a group of spherical particles that share the same properties. The Lagrangian tracking makes it easier to model a distribution of particle sizes of the dispersed phase which would have to be treated as separate phases using the Eulerian technique.

The Newton's second law of motion is solved for the dispersed liquid particles. The drag force, defined by (1), is the force acting on a single parcel due to the relative velocity

between the particle and the continuous surrounding fluid in a uniform pressure field without relative acceleration.

$$F_D = \frac{1}{2} C_D \rho_C A_P |v_{rel}| v_{rel} \tag{1}$$

where C_D is the drag coefficient of the particle, ρ is the density of the continuous phase, v_{rel} is the relative velocity and A_p is the projected area of the particle.

The interaction between the dispersed phase and the continuous phase was simulated as two-way coupling, i.e. both phases can influence to each other exchanging momentum and energy in this case. Condensation and evaporation of the discrete particles was not taken into account in this numerical model.

The simulations were run fully turbulent where the Reynolds averaged Navier-Stokes (RANS) equations were solved with the k-ω SST shear stress turbulence model developed by Menter [21], where the turbulent kinetic energy, k, and the specific dissipation rate, ω, are obtained from the equations (2) and (3).

$$\frac{\partial}{\partial t}(\rho k) + \frac{\partial}{\partial x_i}(\rho k u_i) = \frac{\partial}{\partial x_j}\left(\Gamma_k \frac{\partial k}{\partial x_j}\right) + G_k - Y_k \tag{2}$$

$$\frac{\partial}{\partial t}(\rho w) + \frac{\partial}{\partial x_i}(\rho w u_i) = \frac{\partial}{\partial x_j}\left(\Gamma_w \frac{\partial w}{\partial x_j}\right) + G_w - Y_w + D_w$$
$$\tag{3}$$

To model droplet impingement in a Lagrangian Multiphase simulation it was necessary to set up a Film-Lagrangian phase interaction. Choosing the fluid film model as the interaction mode ensured that all droplets which impinge on the interface of the airfoil were converted to the fluid film. The fluid film model required the creation of a shell region in the space within which the fluid film flows to account for transport and conserved quantities within the film and its interaction with

surroundings. The CFD code assumes that the fluid film is modeled on the surfaces of a volume that contains a background fluid. While the background fluid occupies a regular region, the fluid film must flow in a three dimensional shell region. Thus, a one-cell thickness was defined into the CFD code to convert the initial 2D mesh into a 3D mesh. This fluid film that resides in the surface of the airfoil can form droplets in a process called film stripping. Two models were implemented to simulate this effect, wave film stripping model and edge film stripping, respectively. Wave film stripping models the ejection of droplets from the fluid film as a result of wave-induced instabilities whereas the edge film stripping models the ejection of droplets from the fluid film when it flows over a sharp edge, in this case the trailing edge of the airfoil.

C. Initial and Boundary conditions

A free stream velocity of 30 m/s was defined at the outside, equivalent to a Reynolds number of $2 \cdot 10^6$. Three different cases were studied where the direction of the external airflow corresponds to an angle of attack of 0, 4 and 6 degrees, respectively. Slip boundary condition was defined for both front and back boundaries.

Particles, in this case liquid droplets, enter the computational domain through injectors at three discrete locations as can be seen in Fig. 4. These injectors determine the size, the mass and the velocity distribution of the particles in their initial condition (See Table II)
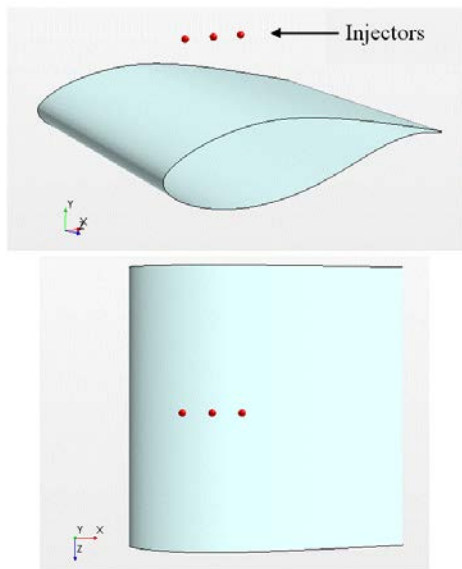

Fig.4 Position of the particle injectors

Injectors properties	
Injector Type	Solid Cone
Outer Cone Angle (°)	30
Mass Flow Rate (kg/s)	0.01
Droplet Diameter (mm)	0.3
Velocity Magnitude (m/s)	30

Table. II Properties of the three injection points

IV. NUMERICAL RESULTS

Continuous phase calculations were considered converged with a three-order-of-magnitude drop in numerical residuals.

Once the continuous phase reached this convergence values the solution was saved to use it as initial condition to start the rain injection. Lift and drag coefficients of the airfoil were used as a measure of performance, which are defined by (4) and (5).

$$C_L = \frac{F_L}{0.5 \cdot A \cdot \rho \cdot v^2} \tag{4}$$

$$C_D = \frac{F_D}{0.5 \cdot A \cdot \rho \cdot v^2} \tag{5}$$

Where F_L and F_D are the lift and drag forces, v is the magnitude of farfield velocity, A is the unit reference area and ρ is the air density.

In HAWT applications, in order to produce more power while reducing the load on the wind turbine structure, it is generally positive to have higher lift force while keeping the drag force as low as possible. The numerical lift and drag coefficient values were calculated for angles of attack of zero, four and six degrees, as shown in Table III. Fig. 5 illustrates the evolution of lift coefficients for each angle attack.
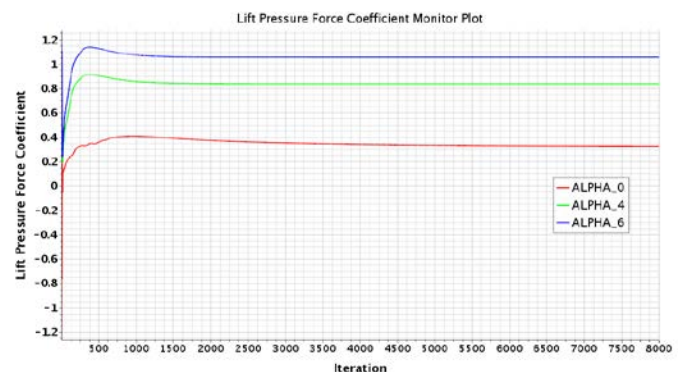

Fig.5 Lift coefficient due to the pressure

DU 91-W2-250		
Alpha (α)	C_L	C_D
0	0.3252	0.0145
4	0.8014	0.0157
6	1.0155	0.01744

Table. III Lift and drag coefficients for each angle of attack

Once the single-phase airflow was converged and the lift and drag values calculated and validated with experimental data, the pressure and velocity distributions along the airfoil were obtained. Then, the multiphase simulation, coupling the single-phase airflow and the dispersed water droplets, was set to calculate the interaction of the fluid film formed due to the impingement and stripping of the water droplets for each angle of attack.

A. Alpha = 0 degrees

The results of this subsection correspond to an angle of attack of zero degrees. Fig. 5 shows the pressure values along the airfoil. As expected, the pressure is larger in the lower part than in the upper surface.
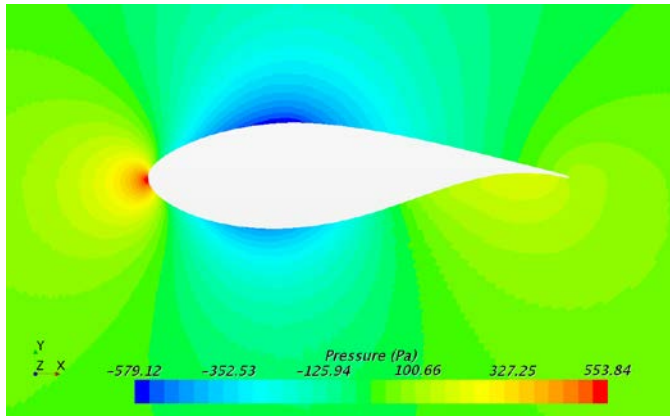

Fig.5 Pressure distribution along the airfoil

A scalar field function, given by (6), was created to determine the amount of mass in the fluid film in each cell.

$$m = \left(\delta_{film} \cdot A\right) \cdot \rho \tag{6}$$

where m is the mass of the fluid film, δ_{film} is the fluid film thickness, A is the area covered by the fluid film and ρ the water density. The result of this field function can then be checked to visualize the mass accumulated locally in the fluid film over time as illustrated in Fig. 6.
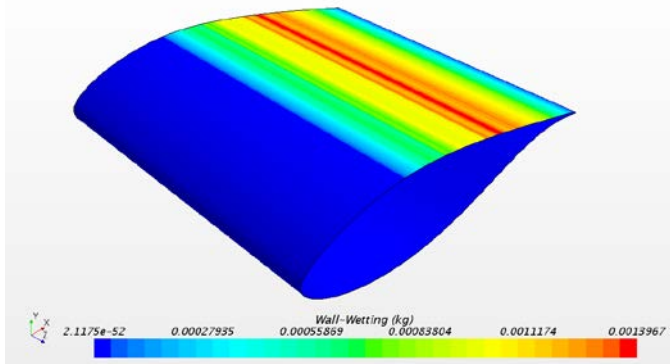
Fig.6 Mass distribution in the fluid film over the airfoil

Fig. 7 illustrates the thickness of the fluid film over the upper part of the airfoil at the time of 3.5 seconds. Note that at this running time the largest thickness of the fluid film is located near the trailing edge. Stripped particles are expected to appear off the film once the fluid film reaches the trailing edge. Edge film stripping models the ejection of droplets from the fluid film when it flows over a sharp edge as in this case.
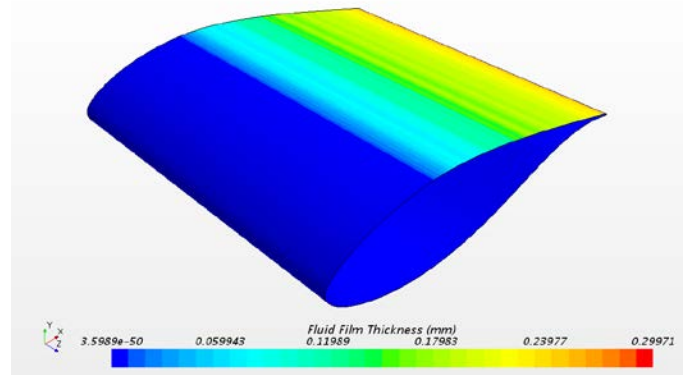

Fig.7 Fluid film thickness after 3.5 s of the water injectors definition.

The pressure coefficient, cp, was also calculated in the airfoil and compared in rain and no-rain conditions, as can be shown in Fig. 8. The cp is a dimensionless number which describes the relative pressures throughout a flow field in fluid dynamics given by (7):

$$C_P = \frac{p - p_\infty}{0.5 \cdot \rho_\infty \cdot V_\infty^2} = \frac{p - p_\infty}{p_0 - p_\infty} \tag{7}$$

where p is the static pressure at the point at which pressure coefficient is being evaluated, p_∞ is the static pressure in the freestream, p_0 is the stagnation pressure in the freestream, ρ_∞ is the freestream fluid density and V_∞ is the freestream velocity of the fluid.

The shape of the cp curves is coherent with the case study of a DU91W(2)250 airfoil. However, some slight differences are visible due to the water droplets impingement on the surface.
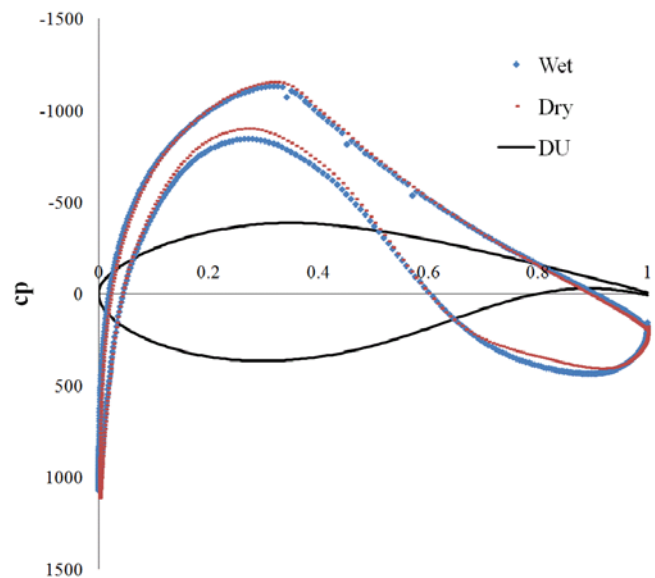

Fig.8 Pressure coefficient curves with no-rain (dry) and rainy (wet) conditions for an angle of attack of zero degrees.

B. Alpha = 4 degrees

Similarly, the effect of the droplets impingement on the airfoil surface was studied with an angle of attack of four degrees. Fig. 9 shows the mass water distribution due to the fluid film formed along the airfoil.
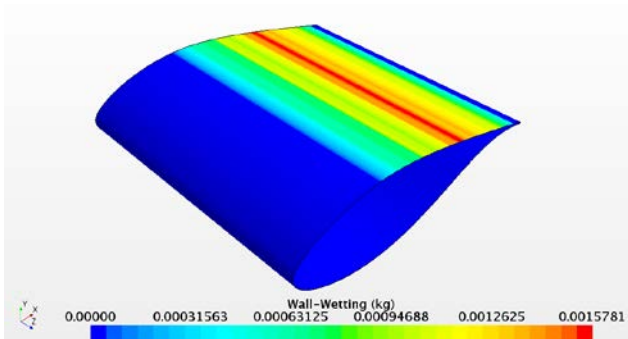

Fig.9 Mass distribution in the fluid film over the airfoil

The fluid film thickness is shown in Fig. 10. As opposed to the case with an angle of attack of zero degrees, the water film does not reach the trailing edge at the time of 3.5 seconds.
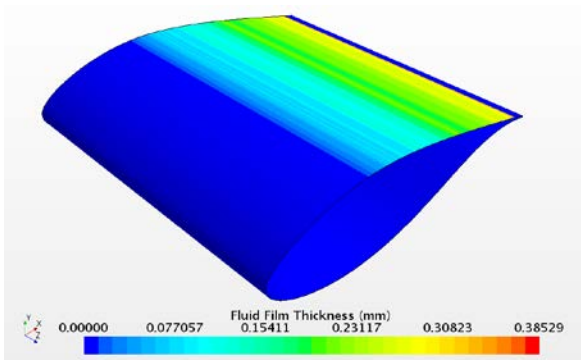

Fig.10 Fluid film thickness after water injectors' definition

With an angle of attack of four degrees, the velocity gradients near the trailing edge region close to the airfoil are smaller in comparison with those formed with an angle of attack of zero degrees, as can be seen in Fig. 11.
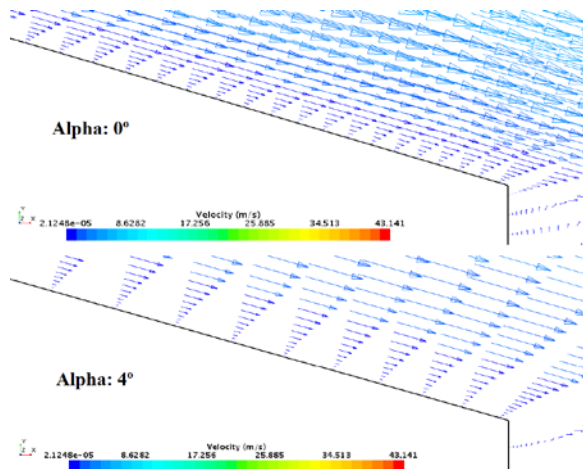

Fig.11 Distribution of velocity gradients near the trailing edge

The shape of the cp curves in dry and wet conditions can be seen in Fig. 12. The difference is not noticeable in comparison with the case with an angle of attack of zero degrees. Some slight differences can be seen in the upper surface, close to the region of impingement of water droplets.
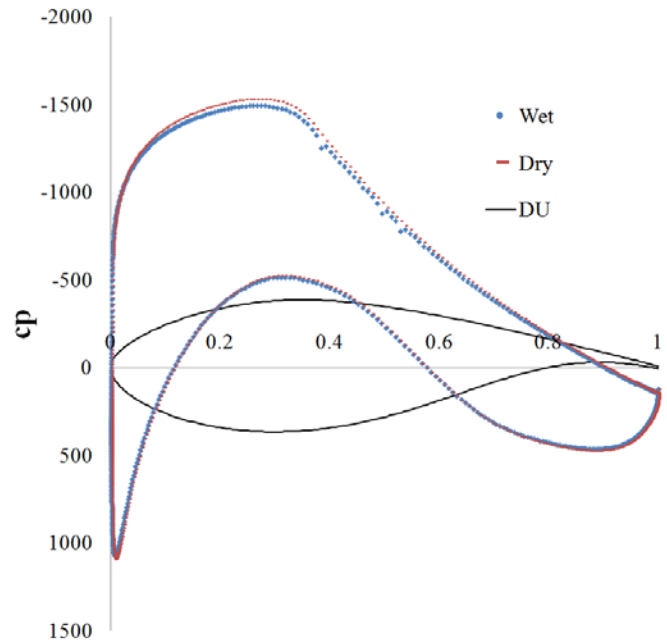

Fig.12 Pressure coefficient curves with no-rain (dry) and rainy (wet) conditions for an angle of attack of four degrees.

C. Alpha = 6 degrees

The results of the amount of mass accumulated in the fluid film over the airfoil are illustrated in Fig. 13 for an angle of attack of six degrees.
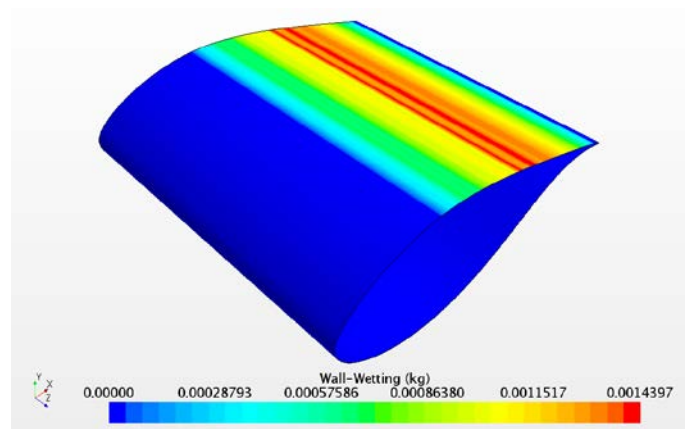

Fig.13 Amount of mass accumulated in the fluid film over time

The fluid film thickness formed over the airfoil due to the droplet impingement is shown in Fig. 14.
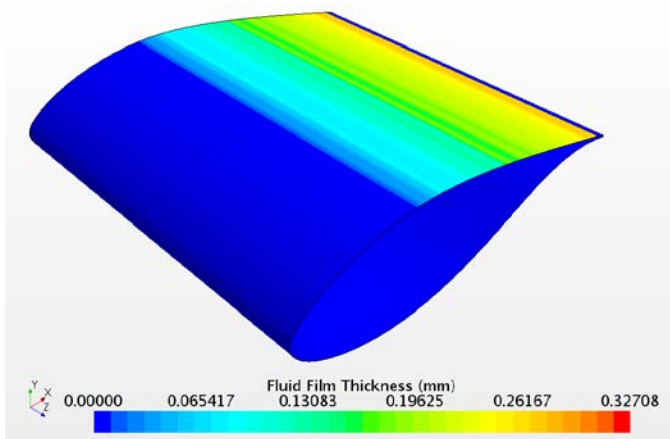
Fig.14 Fluid film thickness after 3.5 s of the water injectors definition (angle of attack six degrees)

The shape of the cp curves is illustrated in Fig. 15 for dry and wet conditions. Fewer differences can be noticed in comparison with the previous cases with zero and four degrees of angle of attack.
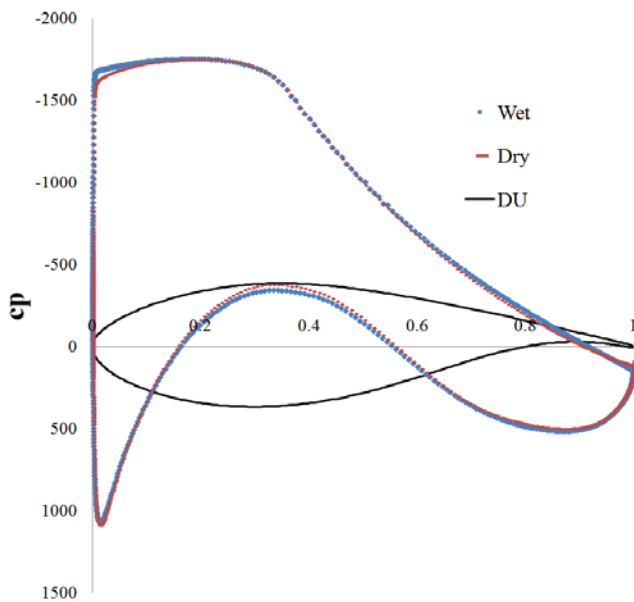

Fig.15 Pressure coefficient curves with no-rain (dry) and rainy (wet) conditions for an angle of attack of six degrees.

V. CONCLUSION

The Lagrangian Multiphase Models along with the definition of multiphase interactions successfully simulate the impingement and fluid film formation of water droplets over an airfoil. The slight difference of the pressure coefficient curves in both case studies confirms that rainy conditions cannot be neglected to study the airfoil aerodynamic performance.

For subsequent studies would be of interest to reduce the s of airfoil section in order to decrease the cell aspect ratio in the mesh generation. This factor, along with the activation of the stabilized film thickness equation, will help to improve

convergence issues due to high mass impingement upon very small fluid film cells.

Further work is also necessary to evaluate the energy losses at higher rainfall rates and at different degrees of angles of attack. Experimental studies will be also of importance in order to validate the results and to improve new numerical models.

It will be also of interest the study of these effects on airfoils with passive and active flow control devices such as vortex generators, microtabs or Gurney flaps. Then, a comparison could be made to evaluate the severity of the fluid film formed along the airfoil with different devices or different airfoil profiles.

REFERENCES

[1] WindEurope, *Wind in Power: 2016 European statistics*, Available: https://windeurope.org/wp-content/uploads/files/about-wind/statistics/WindEurope-Annual-Statistics-2016.pdf

[2] I. Aramendia, U. Fernandez-Gamiz, J. Sancho and E. Zulueta, "State of the art of active and passive flow control devices for wind turbines," in DYNA, vol. 91, 2016, pp. 512-516.

[3] O. Parent and A. Ilinca, "Anti-icing and de-icing techniques for wind turbines: critical review," in *Cold Regions Science and Technology*, vol. 65, 2011, pp. 88-96.

[4] R.V. Rhode, "Some effects of rainfall on flight airplanes and on instrumental indications," *NASA TN-903*, 1941.

[5] J.K. Luers and P.A. Haines, "The effect of heavy rain on wind shear attributed accidents," in *Proceedings of the 19th Aerospace Sciences Meeting*, Paper 81-0390, 1981.

[6] R.J. Hansman Jr. and M.F. Barsotti, "The aerodynamic effect of surface wetting effects on a laminar flow airfoil in simulated heavy rain," in *Journal of Aircraft,* vol. 22, no.12, 1985, pp. 1049-1053.

[7] G.M. Bezos, R.E. Dunham Jr., G.L. Gentry and W. Edward Melson Jr., "Wind tunnel aerodynamic characteristics of a transport-type airfoil in simulated heavy rain environment" *NASA Technical Paper*, 1992.

[8] R.E. Dunham Jr, "The potential influence of rain on airfoil performance. Influence of environmental factors on aircraft wing performance. *Von Karman Institute for Fluid Dynamics, Lecture Series 1987-03.* Rhode-Saint-Genese, Belgium, 1987.

[9] B.C. Al, C. Klumpner and D.B. Hann, "Effect of rain on vertical axis wind turbines" in In Proc. International Conference on Renewable Energies and Power Quality (ICREPQ'11), Spain, 2011, pp. 1263-1268.

[10] C. Siddons, C. Macleod, L. Yang and M. Stack, "An experimental approach to analyzing rain droplet impingement on wind turbine blade materials," in *EWEA Annual Event,* 2015.

[11] J.R. Valentine and R.A. Decker, "A Lagrangian-Eulerian scheme for flow around an airfoil in rain," in *International Journal of Multiphase Flow*, vol. 21, no. 4, 1995, pp. 639-648.

[12] J.R. Valentine and R.A. Decker, "Tracking of raindrops in flow over an airfoil," in *Journal of Aircraft,* vol.32, no.1, 1995, pp. 100-105.

[13] Z. Wu, Y. Cao, and M. Ismail, "Numerical simulation of airfoil aerodynamic penalties and mechanisms in heavy rain," in *International Journal of Aerospace Engineering*, vol. 2013, Ed. Hindawi Publishing Corporation.

[14] M. Cai, E. Abbasi and H. Arastoopour, "Analysis of the performance of a wind turbine airfoil under heavy-rain conditions using a multiphase computational fluid dynamics approach," in *Industrial and Engineering Chemistry Research*, vol.52, no. 9, 2013, pp. 3266-3275.

[15] A.C. Cohan and H. Arastoopour, "Numerical simulation and analysis of the effect of rain and surface property on wind-turbine airfoil performance," in International Journal of Multiphase Flow, vol. 81

[16] J. Jonkman, S. Butterfield, W. Musial and G. Scott, "Definition of a 5-MW reference wind turbine for offshore system development," *Technical Report NREL/TP-500-38060*; National Renewable Energy Laboratory: Golde, CO, USA, 2009.

[17] U. Fernandez-Gamiz, E. Zulueta, A. Boyano, I. Ansoategui and I. Uriarte, "Five Megawatt wind turbine power output improvements by passive flow control devices," in Energies, vol. 10, no. 6, 2017.

[18] W.A. Timmer and R.P.J.O.M. Van Rooij, "Summary of the Delft University wind turbine dedicated airfoils," in *Journal of Solar Energy Engineering-Transactions of the ASME,* vol. 125, no. 4, 2003, pp. 488-496.

[19] U. Fernandez-Gamiz, E. Zulueta, A. Boyano, J.A. Ramos-Hernanz and J.M. Lopez-Guede, "Microtab design and implementation on a 5 MW wind turbine," in *Applied Sciences*, vol. 7, no. 6, 2017

[20] STAR-CCM+ v.11.06 User's Guide, 2016.

[21] F.R. Menter, "Zonal two equation k-w turbulence models for aerodynamic flows," in *Proc 23rd Fluid Dynamics, Plasmadynamics, and Laser Conf. AIAA*, Orlando, 1993.